Self-Excited Torsional Oscillations under Locked-Wheel Braking: Analysis and Experiments

Chunjian Wang*
chunjiw@clemson.edu
Clemson University – International Center for Automotive Research
4 Research Dr., CGEC, Greenville, SC, 29607, USA

Dr. Beshah Ayalew
beshah@clemson.edu
Clemson University – International Center for Automotive Research
4 Research Dr., Room 342 CGEC, Greenville, SC, 29607, USA

John Adcox
john.adcox@us.michelin.com
Michelin America Research Corporation
515 Michelin Rd, Greenville, SC 29605, USA

Benoit Dailliez
benoit.dailliez@fr.michelin.com
Centre de Technologie Europe, Michelin Corporation
Clermont Ferrand, France

Dr. Tim Rhyne
tim.rhyne@us.michelin.com
Michelin America Research Corporation
515 Michelin Rd, Greenville, SC 29605, USA

Steve Cron
steve.cron@us.michelin.com
Michelin America Research Corporation
515 Michelin Rd, Greenville, SC 29605, USA

Presented at the
September 2014
Meeting of the Tire Society

*Presenter / Corresponding Author

C. Wang, B. Ayalew, J. Adcox, B. Dailliez, T. Rhyne, S. Cron

Self-Excited Tire Torsional Oscillations under Locked-Wheel Braking: Analysis and Experiments

REFERENCE: C. Wang, B. Ayalew, J. Adcox, B. Dailliez, T. Rhyne, S. Cron, " Self-Excited Tire Torsional Oscillations under Locked-Wheel Braking: Analysis and Experiments", submitted for presentation at the 2014 Tire Society meeting and for consideration for publication in the journal *Tire Science and Technology.*

ABSTRACT: This paper analyzes the effect of tire/vehicle parameters, specifically of tire/suspension torsional stiffnesses, on the stability of self-excited tire torsional oscillations during locked-wheel braking events. Using a torsionally flexible tire-wheel model and a dynamic tire-ground friction model, two system models for tire oscillations are considered: with suspension torsional compliance included in one but excluded in the other. Bifurcation analysis is conducted on both systems to derive the effect of tire/vehicle parameters on the stability. For the system without suspension torsional compliance, it is highlighted that the primary cause of unstable self-excited oscillations is the 'Stribeck' effect in tire-ground friction. Based on the parameters obtained experimentally, the bifurcation surface of vehicle velocity with respect to tire/suspension torsional stiffness is also given. The effect of tire/suspension torsional stiffness to the stability of tire torsional oscillation is qualitatively validated via comparisons between locked-wheel braking simulations and experiments with tires with different torsional stiffnesses.

KEY WORDS: Stability analysis, bifurcation analysis, tire torsional oscillation, tire/suspension torsional stiffness

Introduction

Tires are the components through which vehicles interact with the ground and through which the traction/braking force and lateral force are generated. Tire dynamics directly influence the vehicle's handling, traction and braking performance, NVH and safety. In the previous work [1], it was noted that tire torsional dynamics, in particular, could compromise the performance of ABS systems significantly for certain tires with very low torsional stiffnesses. However, the dynamics under locked-wheel braking for such low torsional stiffness tires [2] [1] [3] are rarely studied. In this paper, we will show that during hard braking events without ABS, wheel lock-up leads to self-excited torsional oscillations on the tire, especially on low torsional stiffness tires, which become stable/unstable depending on the tire and suspension parameters. These self-excited torsional oscillation on tires were observed indirectly via measurements of brake torque and longitudinal force under locked-wheel braking experiments in [4]. In this work, we

provide an analytical explanation as well as experimental observations by direct measurement of the oscillations on the outer-ring/belt of the tire.

In the literature, it has been observed that the self-excited oscillations of the tire may lead to irregular wear of tire [5, 6], reduced ride quality [7] and/or reduced braking performance[1]. Broadly, self-excited oscillation is a common phenomenon in many applications involving sliding friction [8, 9]. As an example, in [10], the stability and local bifurcation behavior of a friction oscillator due to exponentially decaying friction have been investigated and used to explain the low frequency groan of brake noise. As opposed to static friction models used in [10], a dynamic friction model was used to study the bifurcation of a single-degree-of-freedom mechanical oscillator in [11]. For tires, the paper [12] studied the self-excited lateral oscillation using a piecewise friction model and attributed the polygonal wear of the tire to this oscillation. However, the self-excited torsional oscillation of a tire during locked-wheel braking has not received much attention, partly because of the successful advent of ABS and traction control systems that prevent wheel lock-up. This paper presents a theoretical analysis of the self-excited torsional oscillation under locked-wheel braking in the absence of well-functioning ABSs and provides some experimental observations that support the theoretical analysis.

The analysis of tire torsional oscillation requires appropriate tire and tire-ground friction models. A rigid wheel model, which is used in most traction/ABS controller derivations, is not suitable because the rigid wheel assumption excludes torsional oscillation. In [13] a simple dynamic tire model involving relaxation length concepts was described and validated. Later on, based on this concept, a Rigid Ring Tire Model [4] was proposed which allows analysis of tire vibrations. With the inclusion of the tire modes from in-plane [4] to out-of-plane [14] evolved the commercial dynamic tire model, known as the SWIFT tire model[15]. The use of the SWIFT tire model in braking events included the prediction of the noise component in the wheel angular velocity signal [16, 17], the study of vehicle behavior on uneven roads[18], and tire shimmy analysis [19]. A complex tire dynamic model, known as FTire proposed in recent years [20, 21], incorporates much more degrees-of-freedom to essentially offer similar capabilities. While these sophisticated models represent the state of the art in tire dynamics modeling,

they are not suitable for the insightful simplifications we seek in order to isolate self-excited oscillations.

As for the tire-ground friction model, Pacejka's $\mu - slip$ friction model [19] is widely used for its good approximation of test data and low computational intensity. However, this friction model is based on steady-state experimental data, and tire torsional oscillation under locked-wheel braking is very much a dynamic phenomenon. In [22], a dynamic tire-ground friction model, which is called Average Lumped Parameter model or simply the LuGre tire model, was presented. This tire-ground friction model includes an internal state which represents the tread dynamics for friction generation. This model and its variants[23, 24] have been found to be quite suitable for analyzing friction induced oscillations in many applications [11, 25-27].

In this paper, we adopt a flexible sidewall tire model [2] which captures the tire torsional oscillation. This is a simplification of Rigid Ring Tire Model to the in-plane torsional dynamics due primarily to tire sidewall torsional flexibility. By coupling this model with the LuGre tire-ground friction model, the stability and local bifurcation of locked-wheel braking events will be analyzed. In addition, the effect of suspension torsional compliance and damping will be studied for their influence on the stability of the self-excited oscillations.

The rest of the paper is organized as follows. Section 2 describes two tire torsional oscillation models, with suspension torsional compliance considered in one but neglected in the other. Section 3 details the analysis of the stability and local bifurcation of the systems, showing that the 'Stribeck' effect in the tire-ground friction is the major cause of the unstable tire torsional oscillation. The effect of tire/suspension torsional stiffnesses on the de-stabilizing velocity is also shown in this section based on the model parameters obtained experimentally. The test rig and determination of these parameters are described in Section 4. In Section 5, the comparison between simulations and test data for tires with different torsional stiffnesses are presented to show the effect of tire/suspension torsional stiffness on the stability of tire torsional oscillations. Finally, conclusions are given in Section 6.

2 Tire Model Adopted For Analysis

2.1 Tire torsional oscillation model without suspension compliance

To focus the analysis on the pure torsional dynamics, the following assumptions are made: We consider one corner of a vehicle, where the vehicle/wheel center is assumed to have a longitudinal velocity v_v during the locked-wheel braking event. Torsional deformation in the tire is assumed to remain in the linear range so that the tire sidewall torsional stiffness K_T and damping coefficient C_T can be taken as constants. The schematic of the flexible sidewall tire model adopted is shown in Figure 1, where J_r is the inertia of ring/belt of the tire and F_Z is tire normal load.

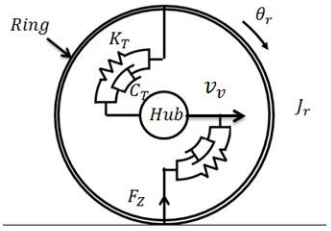

Figure 1: *Flexible sidewall tire model*

We first consider the case where the wheel/hub is supported on a rigid structure (no suspension compliance). The equation of torsional motion for tire ring is given by:

$$J_r\ddot{\theta}_r = F_Z R\mu - K_T\theta_r - C_T\dot{\theta}_r \tag{1}$$

where R is tire radius and the ground friction coefficient is μ. Note that the wheel/hub is assumed locked with applied braking torque.

The LuGre model computes the friction coefficient by [22]:

$$\mu = \sigma_0 z + \sigma_1\dot{z} - \sigma_2 v_r \tag{2}$$

where the relative velocity v_r is

$$v_r = v_v - R\dot{\theta}_r \tag{3}$$

σ_0, σ_1 are parameters representing tread stiffness and damping, σ_2 is the viscous damping which is usually very small and can be approximated as 0. z is the internal state representing tread/bristle deflection and its dynamics is given by:

$$\dot{z} = v_r - \frac{\sigma_0|v_r|}{g(v_r)}z - k\left|\dot{\theta}_r\right|Rz \tag{4}$$

where

$$g(v_r) = \mu_c + (\mu_s - \mu_c)e^{-\left|\frac{v_r}{v_s}\right|^{\alpha}} \tag{5}$$

Coefficient k in (4) is a factor that reflects the tread deflection distribution, and here we adopt the equation from[22]:

$$k = \frac{7}{6} * \frac{1}{L} \tag{6}$$

where L is the length of the contact patch.

During locked-wheel braking, the angular velocity of the ring $\dot{\theta}_r$ can be assumed relatively small compared with vehicle speed v_v, since high slip ratios are involved in this regime.

$$R\left|\dot{\theta}_r\right| < v_v \tag{7}$$

Therefore, according to (3), v_r will be positive in this regime, and

$$|v_r| = v_r \tag{8}$$

By defining $x_1 = \theta_r, x_2 = \dot{\theta}_r$ and $x_3 = z$, the state-space model for the coupled nonlinear system of ground friction and torsionally flexible tire can be assembled as the three-state system:

$$\begin{aligned}
\dot{x}_1 &= x_2 \\
\dot{x}_2 &= \\
&-\frac{K_T}{J_r}x_1 - (\frac{C_T}{J_r} + \frac{F_Z R^2\sigma_1}{Jr} - \frac{F_Z R^2\sigma_2}{J_r})x_2 + \frac{F_Z R\sigma_0}{J_r}x_3 - \frac{F_Z R\sigma_0\sigma_1}{J_r}\frac{(v_v - Rx_2)}{g(v_v - Rx_2)}x_3 - \\
&\frac{F_Z R^2\sigma_1 k}{J_r}|x_2|x_3 + \frac{F_Z R(\sigma_1+\sigma_2)v_v}{J_r} \\
\dot{x}_3 &= -Rx_2 - \sigma_0\frac{v_v - Rx_2}{g(v_v - Rx_2)}x_3 - kR|x_2|x_3 + v_v
\end{aligned} \tag{9}$$

where:

$$g(v_v - Rx_2) = \mu_c + (\mu_s - \mu_c)e^{-\left(\frac{v_v - Rx_2}{v_s}\right)^{\alpha}} \tag{10}$$

Equation (9) can be written compactly as:

$$\dot{X}^H = H(X^H) \tag{11}$$

where $X^H = [x_1 \quad x_2 \quad x_3]^T$, and function H is the vector function representing the right hand side in (9).

2.2 Tire torsional oscillation model with suspension compliance

It is found that in some vehicles the torsional compliance of suspension cannot be neglected as in Section 2.1. So in this section, the wheel/hub will be regarded as supported on torsionally flexible system (instead of a rigid structure) and the equation for the rotational motion of the hub will be added to the existing model. Again, we assume a linear range of this motion of the hub where the torsional stiffness and damping coefficient of the suspension can be regarded as constants. Figure 2 shows the system model with torsionally flexible suspension and a flexible sidewall tire model, where K_{ST} and C_{ST} represent the torsional stiffness and viscous damping for the suspension torsional compliance.

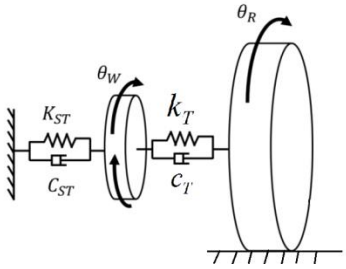

Figure 2: *Flexible sidewall tire supported on a torsional flexible suspension*

The equation of motion for the ring dynamics is modified to:

$$J_r\ddot{\theta}_r = F_Z R\mu - K_T(\theta_r - \theta_w) - C_T(\dot{\theta}_r - \dot{\theta}_w) \tag{12}$$

with the added dynamics of the hub/wheel:

$$J_w\ddot{\theta}_w = K_T(\theta_r - \theta_w) + C_T\left(\dot{\theta}_r - \dot{\theta}_w\right) - K_{ST}\theta_w - C_{ST}\dot{\theta}_w \tag{13}$$

A 5th-order state space model can be assembled combining these equations with the LuGre tire-ground friction model:

$$\dot{X}^G = G(X^G) \tag{14}$$

where the additional states are $x_4 = \theta_w$, $x_5 = \dot{\theta}_w$, X^G is the state vector and $X^G = [x_1\ x_2\ x_3\ x_4\ x_5]^T$, and G is the vector function for the right hand side of the 5th order state space model.

3 Stability and Local Bifurcation Analysis

3.1 The Stribeck effect in tire-ground friction and stability analysis for system without suspension compliance

As indicated by both LuGre friction model [23, 24] and Pacejka's Magic Formula [19], the friction μ decreases with increase of relative velocity. This negative slope is the so-called the Stribeck effect [28] in the tire-ground friction. Figure 3 shows the steady state $(\dot{z} = 0)$ $\mu - slip$ curves obtained from the LuGre model for different vehicle speeds v_v, using values of parameters obtained experimentally (See Section 4) for example tire 2 and listed in Appendix II. Slip ratio s is defined by:

$$\boldsymbol{s = 1 - \frac{R\dot{\theta}_r}{v_v}} \tag{15}$$

Similar curves can be seen in [29]. It can be seen that, in the regime of locked-wheel braking where slip ratio $s \approx 1$, the curves have negative slopes.

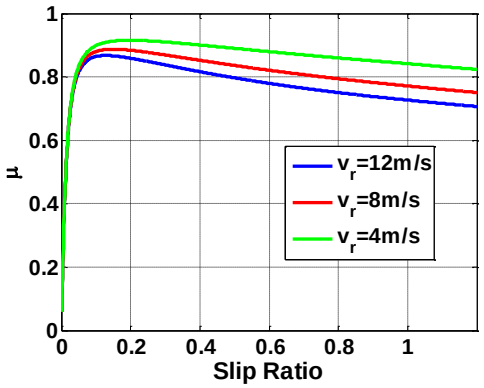

Figure 3: *Steady state $\mu - slip$ curves by LuGre model*

Denoting the local slope at $s \approx 1$ by $-p(v_v)$, at vehicle speed v_v, and the intercept with the μ-axis of a line with this slope by $\mu_i(v_v)$, then the friction coefficient around $s = 1$ may be represented approximately by:

$$\mu(v_v) = \mu_i(v_v) - p(v_v)s \tag{16}$$

for $|s-1| \leq \epsilon$, where ϵ is a small constant.

Plugging (16) with (15) into (1), a simplified equation of motion for the ring is obtained:

$$\ddot{\theta}_r = -\frac{K_T}{J_r}\theta_r + \left(\frac{F_Z R^2 p(v_v)}{v_v J_r} - \frac{C_T}{J_r}\right)\dot{\theta}_r + \frac{F_Z R}{J_r}(\mu_i(v_v) - p(v_v)) \tag{17}$$

It is a linear 2nd-order system and the eigenvalues can be obtained analytically:

$$\lambda = \left(\frac{p(v_v)R^2F_z}{2J_r v_v} - \frac{C_T}{2J_r}\right) \pm \frac{\sqrt{-4J_r K_T v_v^2 + (-p(v_v)R^2F_z + C_T v_v)^2}}{2J_r v_v} \tag{18}$$

The term under the square root is always negative for reasonable values of vehicle load and forward velocity. Then, it can be seen that when $p(v_v) = 0$, which means the Stribeck effect is removed, the real parts of the eigenvalues will be always negative, and there will be no unstable oscillation. It is only with a negative slope in $\mu - slip$ curve, i.e., a positive $p(v_v)$, that the system can have positive eigenvalues and lose stability when the following condition is satisfied:

$$p(v_v)R^2F_z > C_T v_v \tag{19}$$

It can be seen from (19) that in the presence of the Stribeck effect, higher tire load and larger tire effective radius will reduce the stability. It can also be concluded that with certain values of these parameters, the oscillation will become unstable if the vehicle velocity v_v is below a threshold $\frac{p(v_v)R^2F_z}{C_T}$.

It can also be noted from (18) that the sidewall torsional stiffness K_T does not appear in the real part of eigenvalues computed with the steady state friction model, which indicates no effect to the torsional oscillation stability by tire torsional stiffness. In the bifurcation analysis to be discussed later, even if the dynamic friction model used, the effect will be shown to be very minor. However, as will be detailed below, this observation is valid only for the case where suspension torsional compliances are ignored.

3.2 Local bifurcation analysis for the systems with and without suspension compliance

In this section, a local bifurcation analysis is conducted to study the effect tire parameters, specially the torsional stiffnesses, on the stability of the system. For the system without suspension compliance (11), the bifurcation surfaces can be found by setting [30]:

$$H(X^H) = 0 \tag{20}$$

$$\frac{\partial H(X^H)}{\partial X^H}|_{X_0^H} = J^H|_{X_0^H} = 0 \tag{21}$$

From (20) the equilibrium point $X_0^H = [x_{10}^H, x_{20}^H, x_{30}^H]^T$ is obtained, and from (21) the eigenvalues of the Jacobian matrix J^H are set to zero at the equilibrium point. The exact expressions for X_0^H and J^H are given in Appendix I.

By solving (21) for

$$v_v^H = S^H(F_Z, R, K_T, C_T) \tag{22}$$

the bifurcation surface due to F_Z, R, K_T and C_T can be obtained. $v_v^H(F_z, R, K_T, C_T)$ is the de-stabilizing velocity. When $v_v > v_v^H$, the system is stable and the torsional oscillation of the tire is convergent, but when $v_v < v_v^H$, the system become unstable and a divergent tire torsional oscillation can be expected.

Similarly, the equilibrium point X_0^G and Jacobian matrix J^G for system with suspension compliance (14) can be obtained and are given in Appendix I. Then, a similar equation for bifurcation surface of system with suspension compliance (14) can be derived:

$$v_v^G = S^G(F_Z, R, K_T, C_T, K_{ST}, C_{ST}) \tag{23}$$

Given equations as (22) and (23), de-stabilizing velocities v_v with respect to parameters such as F_Z, R, stiffnesses and damping, can be plotted and studied. In this paper, we will focus on the effect of tire torsional stiffness K_T and suspension torsional stiffness K_{ST}.

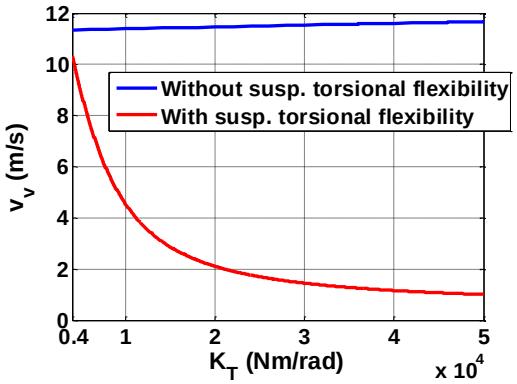

Figure 4: *Bifurcation curve in $v_v - K_T$ plane and comparison between systems with/without suspension torsional flexibility*

Based on parameters obtained in Section 4 and listed in Appendix II, the bifurcation curves in $v_v - K_T$ plane for system with and without suspension torsional compliance are plotted as in Figure 4 (uses parameters for tire 2). It can be seen that in the system without suspension torsional compliance and with dynamic tire-ground friction model used, the de-stabilizing v_v does change with different K_T, but the effect is rather small: magnitude difference of de-stabilizing v_v is only about 0.4m/s when K_T changes from 4000 Nm/rad to 50000 Nm/rad. However, the effect of K_T becomes significant in the presence of suspension torsional flexibility. Besides, in the system without suspension torsional flexibility, higher K_T increases the de-stabilizing v_v, albeit slightly, making the oscillations 'more unstable'; while in the system with suspension torsional flexibility, higher K_T makes the system more stable in locked-wheel braking at normal forward speeds, pushing the threshold speed much lower. The system without suspension torsional flexibility can be regarded as having an infinite suspension torsional stiffness. From this perspective, the observation can also be restated as: lower suspension torsional stiffness K_{ST} improves the effect of K_T on the stability. With an appropriate/realistic choice of K_{ST}, higher K_T is preferred to improve the stability of tire torsional oscillations. This is also supported by the bifurcation surface of v_v due to K_{ST} and K_T, as shown in Figure 5**.**

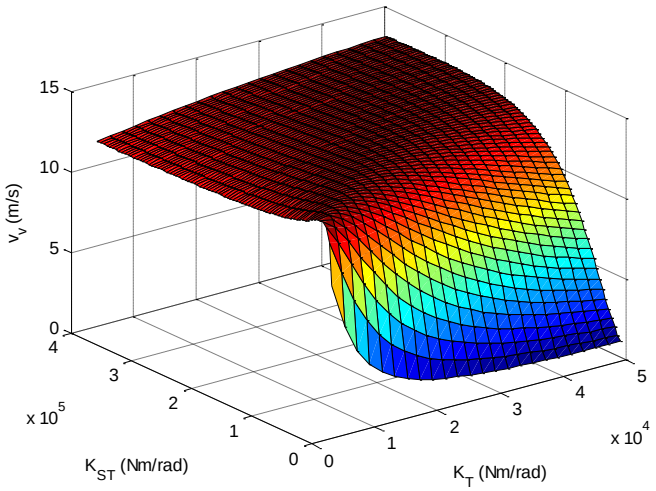

Figure 5: *Bifurcation surface of v_v due to K_{ST} and K_T*

It can be seen from Figure 5 that to minimize the de-stabilizing v_v, higher K_T but lower K_{ST} is preferred. In the area with lower K_{ST}, the de-stabilizing v_v decreases with increase of K_T; but with higher K_{ST}, this trend reverses, which explains and is consistent with the opposite effect of K_T in Figure 4 (increasing de-stabilizing v_v on rigid suspension). Conversely, while with higher K_T, the de-stabilizing v_v increases with K_{ST}; with low K_T, there will be a value for K_{ST} beyond which the de-stabilizing v_v reaches its maximum value (plateaus).

4 Test rig and experimental parameter identification

A test rig similar to that described in [3] is developed for experimental validation of the tire torsional oscillations under locked-wheel braking. A McPherson strut suspension assembly has been installed on the test fixture. A load cell measures the force applied on the suspension, which together with the weight of the suspension assembly, can be used to estimate the normal force at the contact patch F_z. During the test, a chassis dynamometer is used to accelerate the tire to a specified velocity, and then the control mode of chassis dynamometer is switched from velocity control mode to road-load simulation where equivalent vehicle inertia M_{dyno} is specified. The hard-braking torque without ABS is then applied on the brake disc-pad system and is held until the dynamometer stops completely. As shown in Figure 6, a ring velocity sensor that is installed on the strut and attached to the tire ring is used to measure the velocity of the

ring $\dot{\theta}_r$ during the locked-wheel braking event. The wheel speed $\dot{\theta}_w$ and dynamometer speed v_{dyno} are also measured.

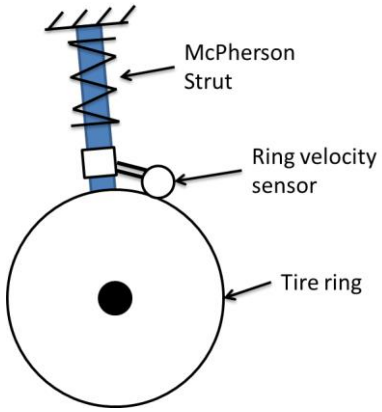

Figure 6: *Ring oscillation measurement*

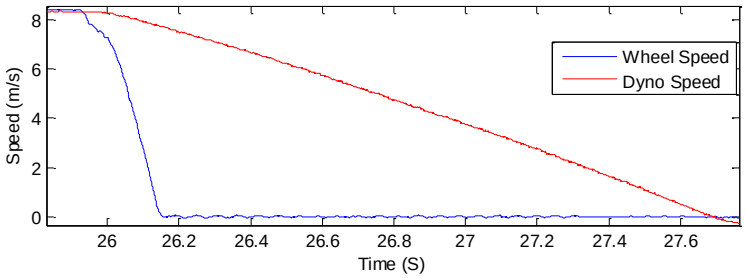

Figure 7: *Measured wheel speed $\dot{\theta}_w$ and dynamometer speed v_{dyno}*

Figure 7 shows a set of measured wheel speed and dynamometer speeds. The equation of the dyno motion can be written as:

$$M_{dyno}\dot{v}_{dyno} = \mu F_z \tag{24}$$

Given an initial speed v_0, $v_{dyno}(t)$ can be represented as a function of friction coefficient μ :

$$v_{dyno}(t) = v_{dyno}(v_0, t, \mu) \tag{25}$$

It is very difficult to measure the friction parameters accurately. In order to get an approximate measurement, we simplify the problem by using a steady-state LuGre friction model, obtained by setting $\dot{z} = 0$. Assuming the ring dynamics $\dot{\theta}_r$ is small enough so that in (4) the coefficient of z:

$$-\left(\frac{\sigma_0|v_r|}{g(v_r)} + k|\dot{\theta}_r|R\right) \approx -\frac{\sigma_0|v_r|}{g(v_r)} \tag{26}$$

Combined with (8), the following relationship can be obtained from model (4):

$$z = \frac{g(v_r)}{\sigma_0} \tag{27}$$

Substitute (23) into (2), the expression for μ is obtained as follows:

$$\mu = g(v_r) = \mu_c + (\mu_s - \mu_c)e^{-\left|\frac{v_r}{v_s}\right|^{\alpha}} \tag{28}$$

We adopted the values for α and v_s from [2] since their estimation requires some sort of a slip control system in the low slip range. Separate investigations by the authors indicate that these values give close fits to measurements on this test rig. Then (25) can be rewritten as:

$$v_{dyno}(t) = v_{dyno}(v_0, t, \mu_s, \mu_c) \tag{29}$$

By solving the model prediction error minimization problem:

$$\min\left(\left[v_{dyno}(\bar{v}_0, t, \mu_s, \mu_c) - \bar{v}_{dyno}(t)\right]^2\right) \tag{30}$$

the best values μ_s, μ_c that fit the experimental data can be obtained. In (30), $\bar{v}_{dyno}(t)$ and $\bar{v}_0$ are, respectively, the measured dynamometer speed and initial speed value. Multiple tests are implemented and the averaged values for μ_s and μ_c are used as the tire-dynamometer friction parameters (given in Appendix II). With the adopted values for σ_0 and σ_1 from [2], a complete characterization of the dynamic LuGre model for tire-dynamometer friction is obtained.

Two tires (numbered tire 1 and tire 2) with different torsional stiffness and damping values are considered here to verify the above-discussed effect of the tire torsional stiffnesses on the stability of the tire torsional oscillation under locked-wheel braking events. It is expected that the friction coefficients are different for different tires. Therefore, we have experimentally identified μ_{s1}, μ_{c1} and μ_{s2}, μ_{c2} for, tire 1 and tire 2, respectively, and listed them in Appendix II.

Torsional stiffness of tire 1 K_{T1}, as well as the torsional stiffness of suspension K_{ST}, are measured from the torsional deformation under controlled torque. The value of

measured K_{ST} on the test rig is listed in Appendix II. It can be seen that this value falls in the low K_{ST} side in Figure 5.

However, tire 2 is a low torsional stiffness tire and is found to have a very nonlinear torsional stiffness, so a nonlinear torsional stiffness curve is obtained by Finite Element Analysis (FEA) for tire2, as shown in Figure 8.

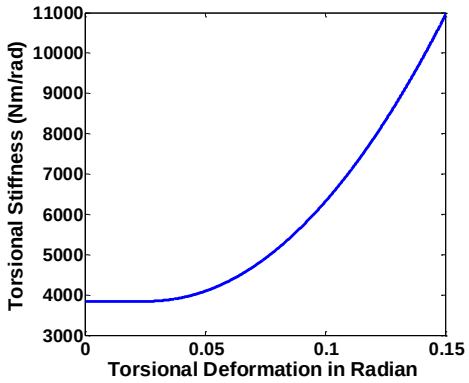

Figure 8: *Nonlinear torsional stiffness of tire 2*

The torsional viscous damping C_T or C_{ST} are obtained via measuring the torsional oscillation response and then curving fitting to the magnitude and phase angle of the response, as shown in Figure 9 which uses parameters for tire 2.

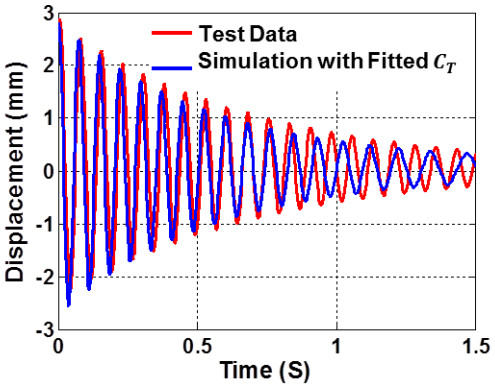

Figure 9: *Measured and fitted oscillation signals for tire 2*

The obtained torsional stiffness and damping values K_{T1} and C_{T1} for tire 1, C_{T2} for tire 2 and K_{ST}, C_{ST} for the suspension torsional compliance are given in Appendix II. It can be seen that tire 2 is much less stiffer than tire 1 but has a little bit higher viscous damping.

5 Comparison between simulations and experiments

The locked-wheel braking tests were conducted on the same suspension and test rig using tire 1 and tire 2. Various signals are recorded and compared with simulation results. The simulation model combining system (14) and dyno dynamics (24) was implemented in Simulink, with the initial condition:

$$v_0 = \dot{\theta}_{r0} R = \dot{\theta}_{w0} R \tag{31}$$

where $\dot{\theta}_{r0}$ and $\dot{\theta}_{w0}$ are the initial velocities of the ring and wheel, respectively.

Figure 10 shows the comparison between simulation and the test data on the dyno velocity v_{dyno} and ring velocity $\dot{\theta}_r R$ for tire 2. It can be seen that the dyno velocity curves are almost on top of each other, which indicates a good fit for the friction parameters, such as μ_{s2}, μ_{c2}. For the ring velocity, both simulation and test data show a rapid drop to around 0, indicating the quick locking of the wheel. The most interesting result is the divergent oscillation in ring velocity after initial convergence. This change in the stability property is also predicted by the simulation result, and corresponding dyno velocity where the oscillation begins to be divergent (de-stabilizing velocity) can also be found to be about 4m/s.

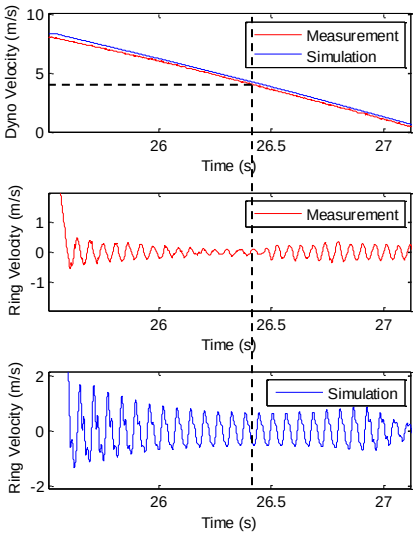

Figure 10: *Comparison between test data and simulation results for tire 2*

As a comparison, tire 1 was used to repeat the experiment and the simulations were re-run with its parameters. Figure 11 shows the comparison between simulation and the test data on the dyno velocity v_{dyno} and ring velocity $\dot{\theta}_r R$ for tire 1. In contrast with tire 2, the ring oscillation is seen to converge quickly in both the test data and simulation after the wheel locked around 25.4s. No divergent oscillation is found when dyno velocity is above 1m/s.

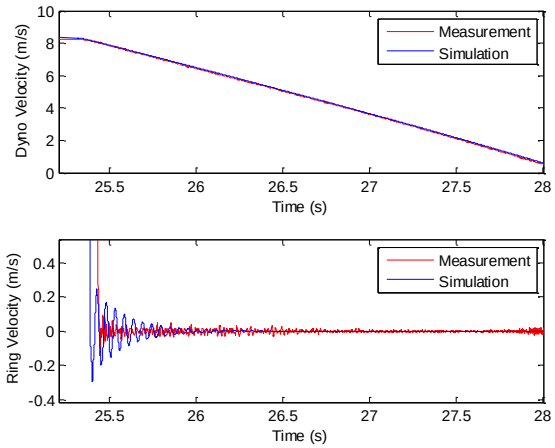

Figure 11: *Comparison between test data and simulation results for tire 1*

From the comparison between results from tire 1 and tire 2, it can be seen that when the tire torsional stiffness is high, the de-stabilizing velocity is reduced from around 4m/s to below 1m/s. This is consistent with the bifurcation analysis results shown in Figure 4 that with the presence of suspension torsional compliance, higher tire torsional stiffness will improve the stability of self-excited tire torsional oscillations and effectively reduce the de-stabilizing velocity to low, easily manageable levels.

6 Summary and Conclusions

This paper analyzed the self-excited tire torsional oscillations under locked-wheel braking. Using a torsionally-flexible tire-wheel model and a LuGre dynamic tire-ground friction model, two overall system models were considered: one with torsionally compliant suspension and another with a torsionally rigid suspension. Stability and bifurcation analysis are conducted to reveal the causes of the instability and the effects of tire and suspension torsional stiffnesses. Using an experimental test rig built around a dyno, the ring speed was measured directly, in addition to wheel speed and dyno speed,

so that the torsional oscillation of the tire could be isolated. Comparative tests were implemented using tires with different torsional stiffnesses. From these analysis and comparisons with test results, the following conclusions can be made:

1) It is shown that the primary cause of the unstable oscillation is the Stribeck effect in tire-ground friction.
2) Without suspension torsional compliance (torsionally rigid suspension), the effect of the tire torsional stiffness on the stability of tire torsional oscillations is very limited. With low suspension torsional compliance, the effect becomes significant, and higher torsional stiffness improves the stability as it reduces the de-stabilizing velocity.
3) The effect of tire torsional stiffness on the stability of the self-excited torsional oscillations is validated via test results on tires with drastically different torsional stiffnesses running on a torsionally flexible suspension.

List of Figure Captions

FIG. 1 - *Flexible sidewall tire model*

FIG. 2 - *Flexible sidewall tire supported on a torsional flexible suspension*

FIG. 3 - *Steady state* $\mu - slip$ *curves by LuGre model*

FIG. 4 - *Bifurcation curve in* $v_v - K_T$ *plane and comparison between systems with/without suspension torsional flexibility*

FIG. 5 - *Bifurcation surface of* v_v *due to* K_{ST} *and* K_T

FIG. 6 - *Ring oscillation measurement*

FIG. 7 - *Measured wheel speed* $\dot{\theta}_w$ *and dynamometer speed* v_{dyno}

FIG. 8 - *Nonlinear torsional stiffness of tire 2*

FIG. 9 - *Measured and fitted oscillation signals for tire 2*

FIG. 10 - *Comparison between test data and simulation results for tire 2*

FIG. 11 - *Comparison between test data and simulation results for tire 1*

Appendix I: Jacobian Matrices

Equilibrium point for system without suspension compliance (11):

$$x_{10}^{H} = \frac{F_Z R g(v_v) - F_Z R \sigma_2 v_v}{K_T}$$

$$x_{20}^{H} = 0$$

$$x_{30}^{H} = \frac{g(v_v)}{\sigma_0}$$

Jacobian Matrix for system without suspension compliance (11):

$$J^H = \begin{bmatrix} 0 & 1 & 0 \\ -\frac{K_T}{J_r} & J_{22} & J_{23} \\ 0 & J_{32} & J_{33} \end{bmatrix}$$

$$J_{22} = \frac{F_Z R^2(\sigma_2 - \sigma_1) - C_T}{J_r} - \frac{F_Z R \sigma_0 \sigma_1}{J_r} x_3[\Phi(x_2)] - \frac{F_Z R^2 \sigma_1 k}{J_r} x_3 \left(\frac{\partial |x_2|}{\partial x_2}\right)$$

$$J_{23} = \frac{F_Z R \sigma_0}{J_r} - \frac{F_Z R \sigma_0 \sigma_1}{J_r} \frac{v_v - R x_2}{\left[\mu_c + (\mu_s - \mu_c) e^{-\left(\frac{v_v - R x_2}{v_s}\right)^{\alpha}}\right]} - \frac{F_Z R^2 \sigma_1 k}{J_r} |x_2|$$

$$J_{32} = -R - \sigma_0 x_3[\Phi(x_2)] - kR x_3 \left(\frac{\partial |x_2|}{\partial x_2}\right)$$

$$J_{33} = -\sigma_0 \frac{v_v - R x_2}{\left[\mu_c + (\mu_s - \mu_c) e^{-\left(\frac{v_v - R x_2}{v_s}\right)^{\alpha}}\right]} - kR|x_2|$$

$$\Phi(x_2) = -\frac{R}{\left[\mu_c + (\mu_s - \mu_c) e^{-\left(\frac{v_v - R x_2}{v_s}\right)^{\alpha}}\right]} - \frac{(v_v - R x_2) \frac{R\alpha}{v_s} \left(\frac{v_v - R x_2}{v_s}\right)^{\alpha - 1} (\mu_s - \mu_c) e^{-\left(\frac{v_v - R x_2}{v_s}\right)^{\alpha}}}{\left[\mu_c + (\mu_s - \mu_c) e^{-\left(\frac{v_v - R x_2}{v_s}\right)^{\alpha}}\right]^2}$$

Equilibrium point for system without suspension compliance (14):

$$x_{10}^{G} = \frac{F_Z R g(v_v) - F_Z R \sigma_2 v_v}{K_T - \frac{K_T^2}{K_T + K_{ST}}}$$

$$x_{20}^{G} = 0$$

$$x_{30}^{G} = \frac{g(v_v)}{\sigma_0}$$

$$x_{40}^{G} = \frac{F_Z R g(v_v) - F_Z R \sigma_2 v_v}{K_{ST}}$$

$$x_{50}^{G} = 0$$

Jacobian Matrix for system without suspension compliance (14):

$$J^G = \begin{bmatrix} 0 & 1 & 0 & 0 & 0 \\ -\frac{K_T}{J_r} & J_{22} & J_{23} & \frac{K_T}{J_r} & \frac{C_T}{J_r} \\ 0 & J_{32} & J_{33} & 0 & 0 \\ 0 & 0 & 0 & 0 & 1 \\ \frac{K_T}{J_w} & \frac{C_T}{J_w} & 0 & -\frac{K_T + K_{ST}}{J_w} & -\frac{C_T + C_{ST}}{J_w} \end{bmatrix}$$

Appendix II: Value of the parameters:

Parameters	Values
$K_{T1}\ [Nm/rad]$	53000
$C_{T1}[Nm \cdot s/rad]$	1.1
$K_{T2}\ [Nm/rad]$	Figure 8
$C_{T2}[Nm \cdot s/rad]$	1.5
$K_{ST}\ [Nm/rad]$	9400
$C_{ST}[Nm \cdot s/rad]$	9
$J_r[kg \cdot m^2]$	0.4
$J_w[kg \cdot m^2]$	0.2
$R[m]$	0.27

$L[m]$	0.2
$F_Z[N]$	2100
$\sigma_0[1/m]$	623
$\sigma_1[s/m]$	1.72
$\sigma_2[s/m]$	0
μ_{s2}	1.0
μ_{c2}	0.6
μ_{s1}	1.1
μ_{c1}	0.75
$v_s[m/s]$	10
α	0.75

References

[1] J. Adcox, B. Ayalew, T. Rhyne, S. Cron, and M. Knauff, "Interaction of Anti-lock Braking Systems with Tire Torsional Dynamics," Tire Science & Technology, vol. 40, pp. 171-85, 07/ 2012.

[2] J. Adcox and B. Ayalew, "Adaptive traction control for non-rigid tire-wheel systems," in ASME 2013 Dynamic Systems and Control Conference, DSCC 2013, October 21, 2013 - October 23, 2013, Palo Alto, CA, United states, 2013, p. Dynamic Systems and Control Division.

[3] J. Adcox, B. Ayalew, T. Rhyne, S. Cron, and M. Knauff, "Experimental investigation of tire torsional dynamics on the performance of an Anti-Lock Braking System," in ASME 2013 International Design Engineering Technical Conferences and Computers and Information in Engineering Conference, IDETC/CIE 2013, August 4, 2013 - August 7, 2013, Portland, OR, United states, 2013, p. Computers and Information in Engineering Division; Design Engineering Division.

[4] P. W. A. Zegelaar, "The Dynamic Response of Tyres to Brake Torque Variations and Road Unevennesses," PhD Dissertation, Delft University of Technology, 1998.

[5] A. Sueoka, T. Ryu, T. Kondou, M. Togashi, and T. Fujimoto, "Polygonal wear of automobile tire," JSME International Journal, Series C, vol. 40, pp. 209-217, 1997.

[6] H.-b. Huang, Y.-J. Chiu, and X.-x. Jin, "Numerical calculation of irregular tire wear caused by tread self-excited vibration and sensitivity analysis," Journal of Mechanical Science and Technology, vol. 27, pp. 1923-1931, 2013.

[7] R. W. Scavuzzo, T. R. Richards, and L. T. Charek, "Tire vibration modes and effects on vehicle ride quality," Tire Science and Technology, vol. 21, pp. 23-39, 1993.

[8] R. A. Ibrahim, "Friction-induced vibration, chatter, squeal, and chaos: Part I - Mechanics of friction," in Winter Annual Meeting of the American Society of Mechanical Engineers, November 8, 1992 - November 13, 1992, Anaheim, CA, USA, 1992, pp. 107-121.

[9] R. A. Ibrahim, "Friction-induced vibration, chatter, squeal, and chaos: Part II - Dynamics and modeling," in Winter Annual Meeting of the American Society of Mechanical Engineers, November 8, 1992 - November 13, 1992, Anaheim, CA, USA, 1992, pp. 123-138.

[10] H. Hetzler, D. Schwarzer, and W. Seemann, "Analytical investigation of steady-state stability and Hopf-bifurcations occurring in sliding friction oscillators with application to low-frequency disc brake noise," Communications in Nonlinear Science and Numerical Simulation, vol. 12, pp. 83-99, 02/ 2007.

[11] Y. Li and Z. C. Feng, "Bifurcation and chaos in friction-induced vibration," Communications in Nonlinear Science and Numerical Simulation, vol. 9, pp. 633-47, 12/ 2004.

[12] X. Yang, S. Zuo, L. Lei, X. Wu, and H. Huang, "Hopf bifurcation and stability analysis of a non-linear model for self-excited vibration of tire," in 2009 IEEE Intelligent Vehicles Symposium (IV), 3-5 June 2009, Piscataway, NJ, USA, 2009, pp. 843-7.

[13] S. K. Clark, R. N. Dodge, and G. H. Nybakken, An evaluation of string theory for the prediction of dynamic tire properties using scale model aircraft tires: National Aeronautics and Space Administration, 1972.

[14] J. P. Maurice, "Short Wavelength and Dynamic Tyre Behaviour Under Lateral and Combined Slip Conditions," PhD Dissertation, Delft University Press, 2000.

[15] A. J. C. Schmeitz, I. J. M. Besselink, and S. T. H. Jansen, "TNO MF-SWIFT," Vehicle System Dynamics, vol. 45, pp. 121-137, 2007/01/01 2007.

[16] S. T. H. Jansen, P. W. A. Zegelaar, and H. B. Pacejka, "The influence of in-plane tyre dynamics on ABS braking of a quarter vehicle model," in Advanced Vehicle Control (AVEC) 1998, 1998, Netherlands, 1999, pp. 249-61.

[17] J. P. Pauwelussen, L. Gootjes, C. Schroder, K. U. Kohne, S. Jansen, and A. Schmeitz, "Full vehicle ABS braking using the SWIFT rigid ring tyre model," Control Engineering Practice, vol. 11, pp. 199-207, 2003.

[18] A. J. C. Schmeitz, S. T. H. Jansen, H. B. Pacejka, J. C. Davis, N. M. Kota, C. G. Liang, et al., "Application of a semi-empirical dynamic tyre model for rolling over arbitrary road profiles," International Journal of Vehicle Design, vol. 36, pp. 194-215, 2004.

[19] H. Pacejka, Tyre and Vehicle Dynamics: Elsevier Science, 2005.

[20] M. Gipser, "FTire: a physically based application-oriented tyre model for use with detailed MBS and finite-element suspension models," Vehicle System Dynamics, vol. 43, pp. 76-91, / 2005.

[21] M. Gipser, "FTire - The tire simulation model for all applications related to vehicle dynamics," Vehicle System Dynamics, vol. 45, pp. 139-151, 2007.

[22] E. Velenis, P. Tsiotras, C. Canudas-De-Wit, and M. Sorine, "Dynamic tyre friction models for combined longitudinal and lateral vehicle motion," Vehicle System Dynamics, vol. 43, pp. 3-29, 2005.

[23] C. Canudas de Wit, H. Olsson, K. J. Astrom, and P. Lischinsky, "A new model for control of systems with friction," IEEE Transactions on Automatic Control, vol. 40, pp. 419-25, 03/ 1995.

[24] C. Canudas-de-Wit, "Comments on 'a new model for control of systems with friction'," IEEE Transactions on Automatic Control, vol. 43, pp. 1189-1190, 1998.

[25] K. Johanastrom and C. Canudas-de-Wit, "Revisiting the LuGre friction model," Control Systems, IEEE, vol. 28, pp. 101-114, 2008.

[26] L. Freidovich, A. Robertsson, A. Shiriaev, and R. Johansson, "LuGre-model-based friction compensation," IEEE Transactions on Control Systems Technology, vol. 18, pp. 194-200, 2010.

[27] C. Yan and W. Junmin, "Adaptive Vehicle Speed Control With Input Injections for Longitudinal Motion Independent Road Frictional Condition Estimation," IEEE Transactions on Vehicular Technology, vol. 60, pp. 839-48, 03/ 2011.

[28] H. Olsson, K. J. Astrom, C. Canudas de Wit, M. Gafvert, and P. Lischinsky, "Friction models and friction compensation," European Journal of Control, vol. 4, pp. 176-95, / 1998.

[29] C. Canudas-de-Wit, P. Tsiotras, E. Velenis, M. Basset, and G. Gissinger, "Dynamic friction models for road/tire longitudinal interaction," Vehicle System Dynamics, vol. 39, pp. 189-226, 2003.

[30] J. Guckenheimer and P. Holmes, Nonlinear Oscillations, Dynamical Systems, and Bifurcations of Vector Fields: Springer-Verlag, 1997.